Hirosaki Med. J. 61(Suppl.) : S11—S22, 2010

TRANSIENT NEURAL ENERGETICS BY FMRI FOR BRIEF AND LONG STIMULI

Peter Herman[1-3], Basavaraju G. Sanganahalli[1-3], Daniel Coman[1-3], Hal Blumenfeld[2-6] and Fahmeed Hyder[1, 2, 3, 7]

Abstract Neuronal activity mapping of cerebral functions using oxidative energetics has become an accepted functional magnetic resonance imaging (fMRI) technique, termed calibrated fMRI. It requires calculation of oxygen consumption (CMR_{O2}) from blood oxygenation level dependent (BOLD) signal using multi-modal measurements of blood flow (CBF) and volume (CBV). This approach is based on a biophysical model which describes tissue oxygen extraction at steady-state, therefore it is unclear if this conventional steady-state BOLD model can be applied transiently for calculating dynamic CMR_{O2} changes. In particular, it is unknown whether calculation of CMR_{O2} from calibrated fMRI differs between brief and long stimuli. In this study linearity was experimentally demonstrated between BOLD-related components and neural activity. We used multi-modal fMRI (at 11.7T) and neuronal signal measurements of local field potential (LFP) and multi-unit activity (MUA) in α-chloralose anesthetized rats during forepaw stimulation to show that respective transfer functions (of BOLD, CBV, CBF) generated by deconvolution with LFP (or MUA) are time invariant, for events in the millisecond to minute range. Since the transfer functions are time invariant for event-related and steady-state stimuli, it is possible to use calibrated fMRI in a dynamic manner. The multi-modal results allowed assignment of a significant component of the BOLD signal that can be ascribed to CMR_{O2} transients. Here we discuss the importance of minimizing residual signal, represented by the difference between modeled and raw signals, in convolution analysis using multi-modal fMRI and neural signals.

Hirosaki Med. J. **61, Supplement** : S11—S22, 2010

Key words: glia; glucose; glutamate; mitochondria; oxygen transport; signaling

Introduction

Mapping neural activity is widely used in neuroscience. Despite advancements to measure neural activity directly, e.g., with electroencephalography (EEG) or magneto-encephalography (MEG), the techniques still have limited spatial resolution and localization problems[1]. Alternative methods of brain mapping are based on secondary signals which measure the *effect* of the neuronal activity on processes such as changes in blood oxygenation level dependent (BOLD) signal and blood flow (CBF) or volume (CBV). However a more direct measure of brain activity, based on thermodynamic principles, is the energy consumption[2]. The main energy source for brain is glucose which is stoichiometrically oxidized in mitochondria to produce ATP efficiently[3]. At steady-state, cerebral oxygen consumption (CMR_{O2}) is measured with ^{13}C or ^{17}O magnetic resonance spectroscopy (MRS)[4,5] as well as with ^{11}C and ^{15}O positron emission tomography (PET)[6,7]. Since these methods require expensive/radioactive isotopes, alternative ways of CMR_{O2} estimation are being sought.

Functional magnetic resonance imaging (fMRI) is widely used for non-invasive brain activity mapping. It provides an indirect measure of neural activity by sensing hyperemic

[1]Magnetic Resonance Research Center (MRRC), [2]Core Center for Quantitative Neuroscience with Magnetic Resonance (QNMR), Departments of [3]Diagnostic Radiology, [4]Neurology, [5]Neurobiology, [6]Neurosurgery, and [7]Biomedical Engineering, Yale University, New Haven, CT 06520, USA.

Address correspondence and reprint requests to: Fahmeed Hyder / Peter Herman
N143 TAC (MRRC/QNMR), 300 Cedar Street, Yale University, New Haven, CT 06520, USA
Tel: +1-203-785-6205, Fax: +1-203-785-6643, e-mail: fahmeed.hyder@yale.edu / peter.herman@yale.edu

changes with the BOLD signal which has *both* energetic and hemodynamic basis. CMR_{O2} can be calculated by calibrating fMRI with additional measurements of CBF and CBV. The BOLD image-contrast depends on changes of magnetic properties of blood: oxy-hemoglobin is diamagnetic, while deoxy-hemoglobin is paramagnetic[8]. At steady-state, based on the Fick's principle[9], the fractional change of BOLD signal ($\Delta S/S$) is given by

$$\Delta S/S = A\left(\frac{\Delta CBF/CBF - \Delta CMR_{O2}/CMR_{O2}}{1+\Delta CBF/CBF} - \Delta CBV/CBV\right) \quad (1)$$

where A is a magnetic field dependent constant and the biophysical and physiological basis of Eq. 1 have been previously described[10,11]. Therefore high spatial resolution CMR_{O2} maps can be obtained by calibrated fMRI using multi-modal but concurrent measurements of BOLD, CBF, and CBV, where each parameter is measured independently (in the same session) with different MRI contrasts (i.e., BOLD with gradient or spin echo; CBF with arterial spin labeling; CBV with exogenous contrast agent). Furthermore the calculated CMR_{O2} can be validated by comparison with MRS or PET measurements[13-15].

An alternative for *dynamic* calibrated fMRI is to test the linearity of the multi-modal signals with neural activity for short and long stimuli. If the strength of each BOLD-related component in Eq. 1 is demonstrated to be linear with neural activity across various stimulus durations, then the respective transfer functions generated by deconvolution with the neural signals should be time invariant, i.e. the transfer function will not depend on the stimulation duration, and thus used for calculating CMR_{O2} dynamics. For CMR_{O2} transients associated with neural events, underlying BOLD-related components were measured and combined with electrophysiology data, over a range of stimuli. Transfer functions generated for brief stimuli with convolution analysis were successfully used to model responses for long stimuli within the range of the uncertainty of experimental measurements[12].

Materials and Methods

Animal preparation and stimulus presentation

All experiments were conducted on artificially ventilated (1-2% halothane during surgery, plus 70%N_2O/30%O_2) adult male rats (n = 26; Sprague-Dawley; 200-300 g; Charles River, Wilmington, MA). Femoral artery and vein were cannulated respectively for monitoring physiologic parameters (pCO_2, pO_2, pH, blood pressure) and for infusion of iron oxide contrast agent for measuring CBV changes[13]. The α-chloralose (~40 mg/kg/h) and D-tubocurarine chloride (~0.3 mg/kg/h) were administered intraperitoneally. Stimulus parameters consisted of 2 mA amplitude pulses of 0.3 ms duration where multiple pulses were separated by 333 ms and the number of pulses varied from 1 to 90. A resting period of 300 s was allowed between repeated stimulation trials (at least four trials per rat: two repetitions per forepaws).

Electrophysiology and CBF

The first group of rats (n = 12) were mounted on a stereotaxic frame and small burr holes were drilled for insertion of adjacent electrical and laser-Doppler flowmetry (LDF) probes to simultaneously measure neural and CBF signals[16]. Although arterial spin labeling (ASL) MRI is used to provide quantitative CBF measurements at steady-state, we used LDF for dynamic CBF measurements because ASL techniques loose perfusion sensitivity at higher temporal resolution[17]. Recordings were localized to middle cortical layers (4.4 mm lateral, 1.0 mm anterior to bregma, 0.9±0.1 mm depth from cortical surface) and confirmed histologically[16,18] for comparison with fMRI signals at the same depth. The scalp was used as the reference and ground for extracellular recordings. Local field potential (LFP) and multi unit activity (MUA)

were obtained by splitting the extracellular data into low (<150 Hz) and high (0.4-10 kHz) bands. Magnitude of the LDF data was calibrated to CBF collected with ASL MRI (3 Hz, 2 mA, 0.3 ms, >90 pulses)[17]. Electrical and optical signals were digitized with CED μ-1401 using Spike 2 software (Cambridge Electronic Design, Cambridge, UK) at 20 kHz and 50 Hz, respectively. To compare with lower temporal resolution BOLD and CBV data, we averaged the raw neural data by running 0.02 s bins.

Multi-modal fMRI

In the second group of rats (n = 14) all fMRI data were obtained on a modified 11.7T Bruker horizontal-bore spectrometer (Bruker, Billerica, MA) using a ^{1}H surface coil radio-frequency probe (1.4 cm diameter) with conventional methods for BOLD and CBV contrasts[19,20]. We used echo-planar imaging (EPI) with sequential sampling[21] and repetition and gradient echo times of 1000 and 15 ms, respectively[17]. We used center-of-mass analysis[22] on all fMRI data to eliminate data sets with movement artifacts.

Estimating parameters of gamma-based transfer functions

The transfer function, $h(t)$, can be computed by deconvolution between the input signal, $i(t)$, and the output signal, $r(t)$. The LFP (or MUA) was used as the input signal, $i(t)$, whereas the BOLD, CBV, and CBF responses each was used as an independent response, $r(t)$. It can be shown that

$$i(t) \otimes h(t) = r(t) \tag{2}$$

where t is time.

The gamma variate function is widely used for modeling transfer functions[23-25]. Since the original form of the equation has some undesirable mathematical properties, we used a slightly different form where the parameters are independent of each other[26],

$$y(t) = y_0 + y_m \left(\frac{t}{t_m} e^{1-\frac{t}{t_m}} \right)^{\alpha} \tag{3}$$

where y_0 is the baseline shift, y_m is the magnitude of the peak, t_m is the peak time, and α is related to the rise and fall times while the appearance time is fixed to zero.

The BOLD and CBF impulses are single gamma variate functions, whereas the CBV impulse is described by two additive gamma variate functions, with fast and slow components. As a result of this dual property, the CBV impulse rises fast, nearly similarly as the BOLD and CBF impulses, but its tail decays slowly requiring more than 30 s to reach the pre-stimulation baseline compared to 4-8 s required for the other two transfer functions. The gamma variate function parameters (y_m, t_m, α) of BOLD and CBF impulses are 0.0061, 2.5637, 2.3518 and 0.1131, 1.8339, 3.896 respectively. The fast component of the CBV impulse has the parameters of 0.058, 2.0595, 3.2279, while the slow component is described by 0.0044, 4.9701, 0.4119. The baseline shift (y_0) is 0 in every case.

Calculating the standard deviation of CMR_{O2}

Eq. 1 can be rewritten as follows to describe the connection between CMR_{O2}, CBF, CBV, and BOLD signal

$$m = \frac{f}{v}\left(1 - \frac{1}{A}\ln(s)\right) \tag{4}$$

where $m = 1 + \frac{\Delta CMR_{O2}}{CMR_{O2}}$, $f = 1 + \frac{\Delta CBF}{CBF}$, $v = 1 + \frac{\Delta CBV}{CBV}$, and $s = 1 + \frac{\Delta BOLD}{BOLD}$. Using Eq. 4, we can estimate the uncertainty of CMR_{O2} estimation using error propagation[27,28]. Measured values of CBF, CBV, and BOLD signal along with their respective standard deviations (σ) can be used to analytically describe the time dependent standard deviation of CMR_{O2}. If the measured signals are independent from each other, the error propagation is restricted only

by the standard deviation of each individual measured component. If different components of the measured data (CBF, CBV, BOLD) are correlated, then their covariances with each other are required to be taken into consideration. Towards that end, the covariances of the correlated data were converted into Pearson correlation coefficients[27,28]. To define the error propagation formulas in simple mathematical terms (e.g. multiplication, summation, etc.), Eq. 4 needs to be rearranged into

$$\frac{1}{A}\ln(s) = X\,,$$

$$f\,\frac{1}{A}\ln(s) = Y\,,$$

$$f - f\,\frac{1}{A}\ln(s) = Z\,,\ \text{and}$$

$$\frac{f - f\,\frac{1}{A}\ln(s)}{v} = m$$

which is equivalent to

$$m = \frac{Z}{v} = \frac{f-Y}{v} = \frac{f-fX}{v} = \frac{f - f\,\frac{1}{A}\ln(s)}{v} = \frac{f}{v}\left(1-\frac{1}{A}\ln(s)\right) \quad (5)$$

The following correlation coefficients (ρ) are required to calculate the standard deviation of CMR_{O2}. Correlation between the CBF and the X is given by the parameter r_1, where

$$r_1 = \rho(f, X) = \rho(f, \ln(s)).$$

Correlation between CBF and Y is given by the parameter r_2, where

$$r_2 = \rho(f, Y) = \rho\left(f,\, f\,\frac{1}{A}\ln(s)\right).$$

Correlation between the numerator (Z) and the denominator (v) of Eq. 5 is given by the parameter r_3, where

$$r_3 = \rho(Z, v) = \rho\left(\left(f\left(1-\frac{1}{A}\ln(s)\right)\right), v\right).$$

Using these coefficients, the standard deviation of CMR_{O2} (σ_m) can be described by

$$\sigma_m = \frac{\sqrt{\left(1-2mr_3^2\sigma_v^2\right)\left(\sigma_f^2 + (f-mv)^2 U - 2r_2\sigma_f(f-mv)\sqrt{U}\right) + m^2\sigma_v^2}}{v},$$

where $U = \left(\frac{\sigma_f}{f}\right)^2 + \left(\frac{\sigma_s}{s\ln(s)}\right)^2 + 2\frac{r_1^2}{A}\frac{\sigma_f^2\sigma_s^2}{fs^2\ln(s)}$.

To calculate a transfer function, a least-square mean (Gauss-Newton) fitting method (Matlab, Natick, MA) was used with iterative steps (Fig. 1): a transfer function was created with initial parameters; it was convolved on the input function; a difference between the modeled and the measured response was calculated to create a residual signal. This method is a modification of Newton's method for detecting a function minimum without using second derivatives, thereby minimizing computational load and time. If the modeled response was significantly different from the measured response, then parameters of the transfer function were changed and the process was repeated. The fitting process was usually completed within several hundred iterations. We assumed the residuals to be acceptable if all of their values were within the range of uncertainty of the measured response, given by ± standard deviation (SD) of the raw signal.

Results

We simultaneously measured electrical and CBF signals from the somatosensory cortex using a dual-sensor probe and compared these signals with BOLD and CBV signals (at 11.7T) in the same cortical location. The LFP (or MUA) and imaging signals (BOLD, CBV, CBF) were measured with brief and long forepaw stimuli to assess whether the hyperemic responses were linearly associated with neural activity. Fig. 2 shows a representative single-trial data set with 4 stimulus pulses. The evoked neural response was immediate and short lived in comparison to the imaging signals which lasted at least about 4s.

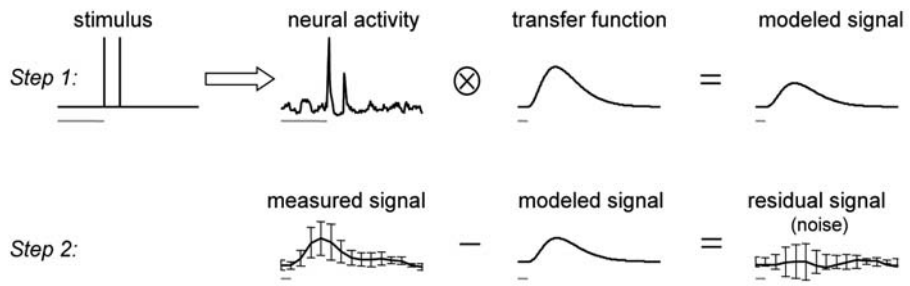

Figure 1 Convolution analysis for calculating transfer functions. For each measured imaging signal (e.g., BOLD, CBV, CBF), a two-step process was utilized to calculate a transfer function which links the measured neural activity (e.g., LFP, MUA) to the measured raw signal. *Step 1*: The stimulus-evoked neural activity convolved with a simulated gamma variate transfer function was used to calculate a modeled signal. *Step 2*: A residual signal (noise) was created by differencing the modeled signal from the measured raw signal. The two steps were iterated until the residual signal (noise) was below ± SD of the measured signal. Only the transfer function was numerically varied during each iterative step following the least-square mean Gauss-Newton fitting method (Matlab, Natick, MA). Less than 300 steps were needed for the convergence between the raw and modeled signals. Data shown for BOLD and LFP with two pulses (2 mA amplitude, 0.3 ms duration) separated by 333 ms. Gray horizontal scale bar is 1 s. (Adapted from Ref #12 with the permission of "John Wiley and Sons".)

Each neural response had two phases (Fig. 2A). A positive phase was initiated immediately after each stimulus pulse which lasted about 150ms. A negative phase, which lasted about 200ms, followed the positive peak. But its amplitude was less than 5% of the initial positive peak, which is well below the SD of the measurement. These positive peaks were used as input signals for the convolution analysis (Fig. 1). Evoked neural responses to multiple stimulus pulses demonstrated a unique pattern (Fig. 2A) which have been noted by others[29] where the alternate responses were attenuated most likely due to inhibitory mechanisms[30] or because of cortical refractory effects[31]. Therefore all subsequent evoked responses were normalized to the first positive component (Fig. 3A). For long lasting stimuli (90 pulses), in addition to the alternating stronger and weaker responses for consecutive stimulus pulses, the magnitude of responses generally decreased during the initial 5-6s to subsequently reach a new plateau (e.g., see Fig. 3A, extreme right). These observations are in good agreement with prior results[32,33].

Amplitudes and time-to-peak of the imaging signals (Figs. 3 B-D) are in good agreement with prior observations[34,35]. The mean time-to-peak of the BOLD response was 3.9±0.3s. The response intensity (and width) gradually increased from 1 to 4 pulses and reached a plateau for 90 pulses (2.9±1.8%, 3.4±1.2%, 4.4±2.1%, 8.02±1.3%, and 7.8±4.2%, respectively). The CBF signals showed similar tendencies. The mean time-to-peak of the CBF response was 3.2±0.2s, whereas the intensities were 51.8±28.2%, 75.1±23.3%, 87.7±23.2%, 100.9±31.1%, and 100.1±37.8%, respectively. The mean time-to-peak in CBV response was 3.3±0.7s and the response intensities gradually increased from 1 to 4 pulses (0.8±1.8%, 3.8±1.2%, 7.6±2.1%, and 9.5±1.4%, respectively). The CBV response for 90 pulses of stimulation after an initial rapid rise (10.8±3.6%) showed a secondary slow increase (15±5%) lasting more than 15s. These temporal characteristics of CBV are typical of red blood cell and plasma volume changes[19]. Using the strength (i.e., both intensity and width) of each evoked signal, neural responses were correlated with the strength of each imaging signal. Increasing number of stimulus pulses augmented responses in each of the signals (Fig. 3E). The so-called Grubbs law[36] (i.e., CBV = CBF^{ϕ}) is critical for calculating dynamic CMR_{O2} from calibrated fMRI[34]. The value of Φ was ~0.15

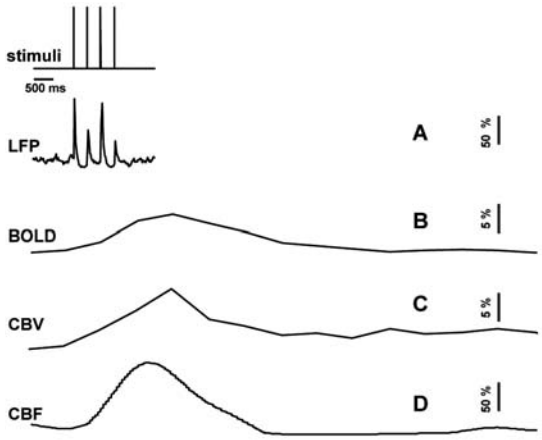

Figure 2 Single trial multi-modal data. Representative neural (A; LFP) and imaging (B-D; BOLD, CBV, CBF) signals for brief forepaw stimuli. While there was an evoked LFP for each stimulus pulse, alternate LFP's were not identical. A similar trend was observed for MUA (data not shown). (Adapted from Ref #12 with the permission of "John Wiley and Sons".)

at the peak of the hyperemic response (Fig. 3F), which is in agreement with prior animal studies[35,37].

Difference between linear and non-linear relationships can be elucidated with a transformation between neural and imaging signals with a transfer function. We applied convolution and fitting methods in an iterative way to find a transfer function relating the neural and imaging signals. The effectiveness of this process was characterized by the residual signal given by the difference between the measured and modeled signals (Fig. 1). In all cases examined, the residual signal was lower than ±SD in measurement of each imaging signal (Fig. 3B-D, bottom traces). For a more thorough inspection for goodness of fit, we averaged the root mean square (RMS) of the residual signal for an entire data set and compared that with the average of measurement SD. In all cases examined, the average value of RMS residual signal was significantly lower than the average values of measurement SD. These results suggest a linear relationship between neural and imaging signals to provide universal transfer functions, applicable for both brief- and long-lasting stimuli. Results of linearity from the convolution analysis, therefore, provides a strong basis for applying Eq. 1 to calculate CMR_{O2} changes (using A = 0.5[16,18] at 11.7T), not only for steady-state stimuli but also for transient events. The calculated CMR_{O2} dynamics in Fig. 4 show experimental evidence of a linear dependency of oxidative energy demanded by neural events and its relationship with CBF. A detailed description of the SD calculation for CMR_{O2} shows that CBF has a dominanting influence and thus the larger SD of CBV has minimal effect on CMR_{O2} uncertainties.

Discussion

The goal here was to calculate CMR_{O2} transients using *dynamic* calibrated fMRI. We used a systematic convolution analysis to find a transfer function between neural activity and each imaging signal, whereas the effectiveness of the impulse response function was portrayed by the residual signal (Fig. 1). If fluctuations of the residual signal were smaller than the uncertainty or SD of the raw signal, the convolution process could produce a universal impulse response function that may be used to model each BOLD-related component successfully for all stimulus parameters. Then linearity between each imaging signal and neural activity will be demonstrated and render the respective transfer functions to be time invariant. Similar trends were observed with LFP or MUA used as the input signal for the deconvolution process (data not shown).

In α-chloralose anesthetized rats, multi-modal fMRI and electrophysiology data (Fig. 2) were evaluated to show that the respective transfer functions (of BOLD, CBV, CBF) generated by convolution with neural activity (LFP or MUA) are indeed time invariant, for *both* brief- and long-lasting events (Fig. 3). It was possible, therefore, to extract a considerable part of the BOLD signal and assign it to dynamic CMR_{O2}

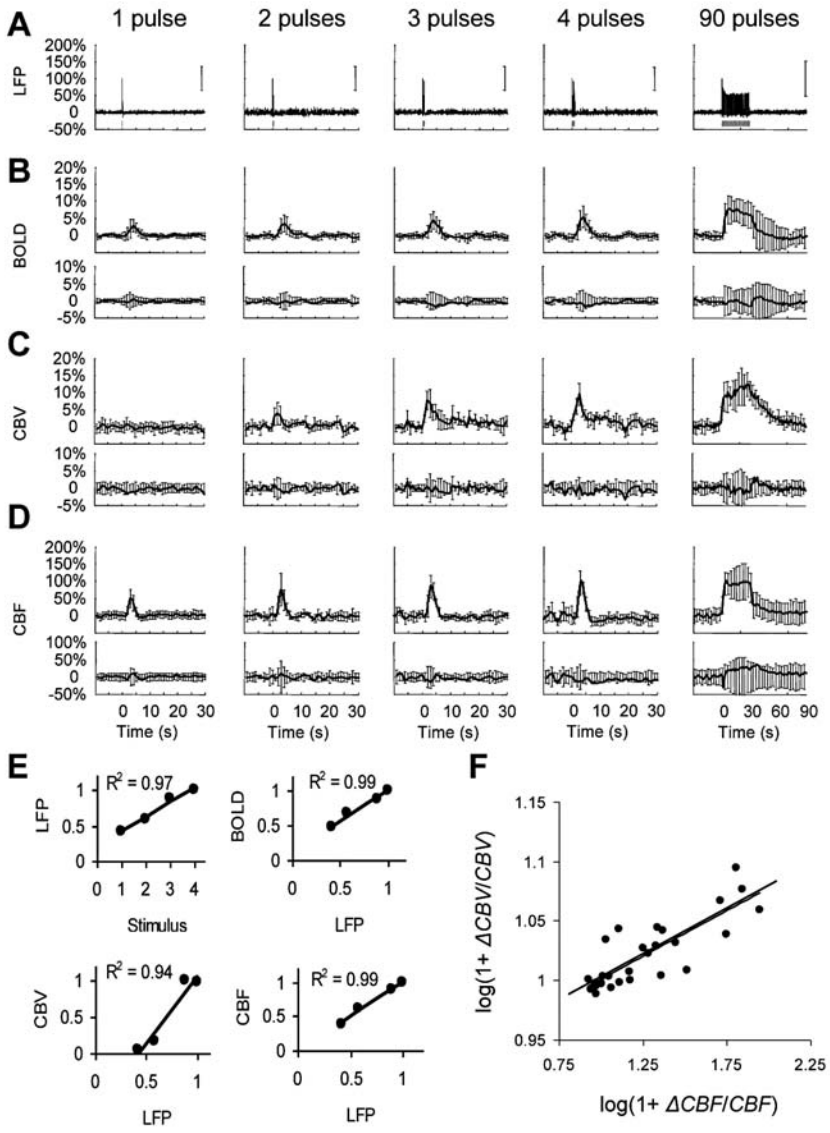

Figure 3 Multi-modal data for brief and long events. Measured neural (A; LFP) and imaging (B-D; BOLD, CBV, CBF, upper rows) signals were used to generate transfer functions. Transfer functions were used to generate modeled signals. The residual signal, created by subtracting the modeled signal from the measured signal, was lower than ± SD of the measured signal (B-D; BOLD, CBV, CBF, lower rows). (E) Relationship between strength (i.e., both intensity and width) of evoked signals. The LFP responses were normalized to the response with 4 stimulus pulses. The BOLD, CBV and CBF data were calculated as normalized by area under the curves. (F) The so-called Grubb's law (i.e., $CBV = CBF^{\Phi}$) given by the slope of the log-log plot of change in CBF and CBV. The data points are from the hyperemic portion for all stimuli with Φ of ~0.08 where the peak values averaged to ~0.15. (Adapted from Ref #12 with the permission of "John Wiley and Sons".)

changes, for stimuli ranging from milliseconds to minute ranges (Fig. 4). Because CMR_{O2} predicted at steady-state by calibrated fMRI had been validated in the past by independent measurements[11], the CMR_{O2} data calculated here for 90 stimulus pulses withstands the same corroboration because ΔCMR_{O2} predicted in our prior and present studies are in good agreement. Given that the exact same transfer functions (of BOLD, CBV, CBF) can be used for modeling signals with few or many stimulus pulses, the CMR_{O2} data validation for longer stimuli can be extended to shorter stimuli, pending independent measurements at this time scale.

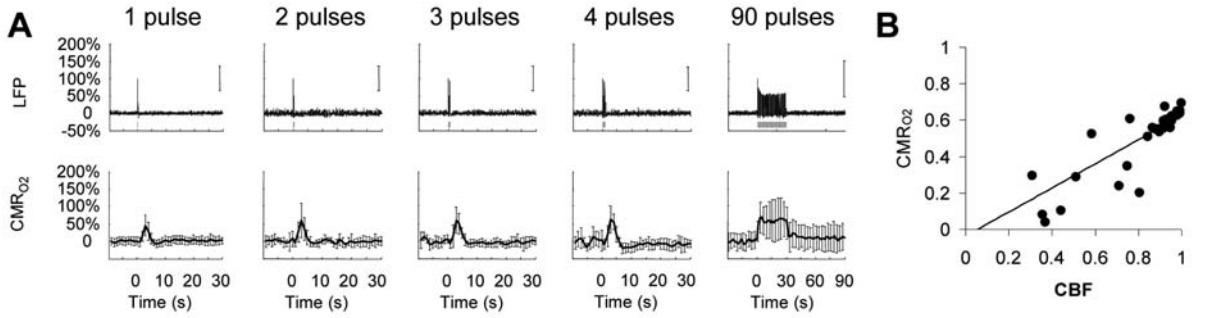

Figure 4 (A) Measured LFP and calculated CMR_{O2} signals for transient to steady-state stimuli. Convolution analysis of the universal transfer functions suggests linearity of the imaging signals with neural activity (Fig. 3E). (B) Coupling between changes in CBF and CMR_{O2} with a linear fit (slope=0.661, interception= -0.039, r^2=0.81). (Adapted from Ref #12 with the permission of "John Wiley and Sons".)

The characteristics of CMR_{O2} responses were similar to CBF changes, but were impacted by CBV dynamics. However because the Φ value (prescribed by Grubb's law: $CBV = CBF^{\phi}$) varied throughout the hyperemic response, we did not use a fixed Φ value for the CMR_{O2} calculation[34].

Results of a convolution are contingent on the choice of the input signal. The stimulus itself is often used as the input when neural activity measures are lacking. However the evoked neural response is preferred because the imaging signals are mechanistically linked to both pre- and post-synaptic events at the nerve terminal[38], not the stimulus itself. Neural activity can be measured invasively (i.e., directly with microelectrodes) or non-invasively (i.e., indirectly with EEG or MEG).

EEG measures summed activity of post-synaptic currents, whereas MEG measures tiny magnetic fields (in fT range) produced by synchronized dendritic activities. EEG and MEG signals originate from slightly different cortical locations and are acquired with different temporal resolutions (ms vs. μs). Since EEG and MEG suffer from the inverse problem (i.e., difficulty localizing origin of signal), the spatial resolution (in cm range) is compromised. EEG signals are susceptible to body movements and MEG signals from the brain sometimes compete with higher magnitude environmental noise. However non-invasive use of EEG and MEG in humans is invaluable for basic science and clinical research[38].

Extracellular recordings (LFP, MUA) typically represent activity from neuronal-glial ensembles in the microelectrode's vicinity, integrating a wide bandwidth of signals spanning short distances in the cortex (μm to mm). Because of the higher spatiotemporal resolution of extracellular recordings, LFP (or MUA) is an obvious candidate for the input signal because each evoked signal in response to a stimulus pulse can be incorporated into the convolution analysis, thereby sensitizing the subtle dynamic nuances of neural activities onto the modeled imaging signals. While evoked signals captured by EEG may appear to be similar in shape and form to LFP, there is greater chance of signal contamination due to noise injection from a variety of sources (e.g., limb movements, breathing, heart beat, etc.)[38].

Because of technical limitations, it is difficult to measure neural and imaging signals from the same exact tissue volume. Therefore our convolution analysis of the multi-modal data acquired within a single "mesoscopic scale" compartment could be termed as a heuristic approach. However multi-compartment oxygen delivery models, which have detailed descriptions of the microvascular bed, take account of

different sampling volumes[39-42] but lack multi-modal experimental data. Therefore future renditions of these oxygen transport models can make use of the multi-modal data availed from our study.

Consistent, and yet peculiar, practices in convolution analysis are smoothing and integration of neural signals. The smoothing (or box-car) approach stems from lumping consecutive stimuli prior to convolution[43,44]. This means that difference between one and two pulses would be double, one and three pulses would be triple, and so on. This approach overlooks attenuation of early vs. late responses during long stimuli (90 pulses). The integration approach is related to interpolating between separate neural events to create the impression of a more *robust* neural signal[25,32,45]. This means that if there were four evoked responses to four stimulus pulses, by integrating between the signals there would be one pseudo box-car to represent the neural signal. For long stimulus durations, the smoothing/integration processes will have minimal impact on the convolution analysis compared to the case if actual neural signals were used. However for shorter stimuli, where the goal is to include subtleties of the neural response variations from moment-to-moment, these practices could generate apparent non-linearity trends.

The *same* universal transfer function is applicable for event related paradigms and steady-state conditions (Figs. 2 and 3) but also for stimuli with higher (6Hz) and lower (1.5Hz) frequencies[31], which is in agreement with prior studies where linearity has been observed with variation of stimulation frequencies using different anesthetics[29,46]. Although different anesthetized (or baseline) states produce different sensory-induced magnitude of responses[47-50], coupling between changes in neural and imaging signals are well correlated. In agreement with our findings, prior studies using a similar stimulation paradigm but different anesthetized conditions have shown that neural activity is coupled with imaging signals using a variety of stimulus durations[46,51].

Prior studies demonstrate non-linearity trends with stimulus amplitude variations[33,45,46,52-54]. Therefore our approach excluded amplitude variations given the narrow dynamic range for testing linearity relationships. Since the transfer functions are dependent on *measured* neural responses and each of the *measured* imaging signals, we expect that the predictions could be applied to other baseline situations, but limited to the somatosensory region.

Factors that affect the BOLD signal include blood hematocrit[8,10,11]. At steady-state, CMR_{O2} calculation by calibrated fMRI assumes that volume (or discharge) hematocrit is unchanged. Under steady-state conditions, this assumption has been partly confirmed by comparing kinetics of red blood cell and plasma volumes[19]. However dynamically different velocities of red blood cell and plasma compartments may become exaggerated in capillaries which in turn could affect the flow (or tube) hematocrit[55]. Therefore an important consideration for future studies is the involvement of transient hematocrit changes[56] on the dynamic BOLD contrast, which may account for some of the small imperfections in the residual signals we have observed.

In summary, we collected multi-modal data consisting of neural and imaging signals and applied convolution analysis (i) to demonstrate linear relationships between neural and imaging signals as well as (ii) to verify the time invariance of their transfer functions. Because these transfer functions could produce modeled signals for brief (1-4 pulses) and long (90 pulses) stimuli successfully, we extended calibrated fMRI for CMR_{O2} calculation, from transient events to steady-state. Results from our laboratory[31] suggest that this approach can be extended for stimuli of varying frequencies. However further

studies are required to understand differences between cortico-cortical and cortico-subcortical regions where neural activity patterns and microvasculature are known to be different[57].

Acknowledgements

This work was supported by NIH grants (R01 MH-067528, R01 NS-049307, P30 NS-52519).

References

1) Srinivasan R, Winter WR, Nunez PL. Source analysis of EEG oscillations using high-resolution EEG and MEG. Prog Brain Res 2006;159:29-42.

2) Hyder F, Rothman DL, Shulman RG. Total neuroenergetics support localized brain activity: implications for the interpretation of fMRI. Proc Natl Acad Sci USA 2002;99:10771-6.

3) Riera JJ, Schousboe A, Waagepetersen HS, Howarth C, Hyder F. The micro-architecture of the cerebral cortex: functional neuroimaging models and metabolism. Neuroimage 2008;40: 1436-59.

4) Hyder F, Patel AB, Gjedde A, Rothman DL, Behar KL, Shulman RG. Neuronal-glial glucose oxidation and glutamatergic-GABAergic function. J Cereb Blood Flow Metab 2006;26:865-77.

5) Zhu XH, Du F, Zhang N, et al. Advanced in vivo heteronuclear MRS approaches for studying brain bioenergetics driven by mitochondria. Methods Mol Biol 2008;489:317-57.

6) Kudomi N, Hayashi T, Teramoto N, et al. Rapid quantitative measurement of CMRO(2) and CBF by dual administration of (15)O-labeled oxygen and water during a single PET scan-a validation study and error analysis in anesthetized monkeys. J Cereb Blood Flow Metab 2005;25:1209-24.

7) Vafaee MS, Gjedde A. Model of blood-brain transfer of oxygen explains nonlinear flow-metabolism coupling during stimulation of visual cortex. J Cereb Blood Flow Metab 2000;20:747-54.

8) Ogawa S, Lee TM, Barrere B. The sensitivity of magnetic resonance image signals of a rat brain to changes in the cerebral venous blood oxygenation. Magn Reson Med 1993;29:205-10.

9) Kety SS, Schmidt CF. The nitrous oxide method for the quantitative determination of cerebral blood flow in man; theory, procedure and normal values. J Clin Invest 1948;27:476-83.

10) Kennan RP, Zhong J, Gore JC. Intravascular susceptibility contrast mechanisms in tissues. Magn Reson Med 1994;31:9-21.

11) Hyder F, Kida I, Behar KL, Kennan RP, Maciejewski PK, Rothman DL. Quantitative functional imaging of the brain: towards mapping neuronal activity by BOLD fMRI. NMR Biomed 2001;14:413-31.

12) Herman P, Sagnganahalli BG, Blumenfeld H, Hyder F. Cerebral oxygen demand forshort-lived and steady-state events. J Neurochem 2009;109:73-79

13) Kida I, Kennan RP, Rothman DL, Behar KL, Hyder F. High-resolution CMR(O2) mapping in rat cortex: a multiparametric approach to calibration of BOLD image contrast at 7 Tesla. J Cereb Blood Flow Metab 2000;20:847-60.

14) Zhang N, Zhu XH, Lei H, Ugurbil K, Chen W. Simplified methods for calculating cerebral metabolic rate of oxygen based on 17O magnetic resonance spectroscopic imaging measurement during a short 17O2 inhalation. J Cereb Blood Flow Metab 2004;24:840-8.

15) Ito H, Ibaraki M, Kanno I, Fukuda H, Miura S. Changes in cerebral blood flow and cerebral oxygen metabolism during neural activation measured by positron emission tomography: comparison with blood oxygenation level-dependent contrast measured by functional magnetic resonance imaging. J Cereb Blood Flow Metab 2005;25:371-7.

16) Schridde U, Khubchandani M, Motelow JE, Sanganahalli BG, Hyder F, Blumenfeld H. Negative BOLD with large increases in neuronal activity. Cereb Cortex 2008;18:1814-27.

17) Kida I, Maciejewski PK, Hyder F. Dynamic imaging of perfusion and oxygenation by functional magnetic resonance imaging. J Cereb Blood Flow Metab 2004;24:1369-81.

18) Englot DJ, Mishra AM, Mansuripur PK, Herman P, Hyder F, Blumenfeld H. Remote effects of focal hippocampal seizures on the rat neocortex. J Neurosci 2008;28:9066-81.

19) Herman P, Sanganahalli BG, Hyder F. Multimodal measurements of blood plasma and red blood cell volumes during functional brain activation. J Cereb Blood Flow Metab 2009;29:19-24.

20) Sanganahalli BG, Herman P, Hyder F. Frequency-dependent tactile responses in rat brain measured by functional MRI. NMR Biomed 2008;21:410-6.

21) Hyder F, Rothman DL, Blamire AM. Image reconstruction of sequentially sampled echo-planar data. Magn Reson Imaging 1995;13:97-103.

22) Chahboune H, Ment LR, Stewart WB, Ma X, Rothman DL, Hyder F. Neurodevelopment of C57B/L6 mouse brain assessed by in vivo diffusion tensor imaging. NMR Biomed 2007;20:375-82.

23) King RB, Deussen A, Raymond GM, Bassingthwaighte JB. A vascular transport operator. Am J Physiol 1993;265:H2196-208.

24) Boynton GM, Engel SA, Glover GH, Heeger DJ. Linear systems analysis of functional magnetic resonance imaging in human V1. J Neurosci 1996; 16:4207-21.

25) Martin C, Martindale J, Berwick J, Mayhew J. Investigating neural-hemodynamic coupling and the hemodynamic response function in the awake rat. Neuroimage 2006;32:33-48.

26) Madsen M. A simplified formulation of the gamma variate function. Phys Med Biol 1992;37:1597-600.

27) Ku H. Notes on the use of propagation of error formulas. J Research of National Bureau of Standards-C. Engineering and Instrumentation 1966;70C:263-73.

28) Bevington PR. Data reduction and error analysis for the physical sciences, New York, McGraw-Hill, Inc., 1969.

29) Matsuura T, Kanno I. Quantitative and temporal relationship between local cerebral blood flow and neuronal activation induced by somatosensory stimulation in rats. Neurosci Res 2001;40:281-90.

30) Hellweg FC, Schultz W, Creutzfeldt OD. Extracellular and intracellular recordings from cat's cortical whisker projection area: thalamocortical response transformation. J Neurophysiol 1977;40: 463-79.

31) Sanganahalli BG, Herman P, Blumenfeld H, Hyder F. Oxidative neuroenergetics in event-related paradigms. J Neurosci 2009;29:1707-18.

32) Ances BM, Zarahn E, Greenberg JH, Detre JA. Coupling of neural activation to blood flow in the somatosensory cortex of rats is time-intensity separable, but not linear. J Cereb Blood Flow Metab 2000;20:921-30.

33) Sheth SA, Nemoto M, Guiou M, Walker M, Pouratian N, Toga AW. Linear and nonlinear relationships between neuronal activity, oxygen metabolism, and hemodynamic responses. Neuron 2004;42:347-55.

34) Kida I, Rothman DL, Hyder F. Dynamics of changes in blood flow, volume, and oxygenation: implications for dynamic functional magnetic resonance imaging calibration. J Cereb Blood Flow Metab 2007;27:690-6.

35) Shen Q, Ren H, Duong TQ. CBF, BOLD, CBV, and CMRO(2) fMRI signal temporal dynamics at 500-msec resolution. J Magn Reson Imaging 2008;27: 599-606.

36) Grubb RL, Jr., Raichle ME, Eichling JO, Ter-Pogossian MM. The effects of changes in PaCO2 on cerebral blood volume, blood flow, and vascular mean transit time. Stroke 1974;5:630-9.

37) Jin T, Kim SG. Cortical layer-dependent dynamic blood oxygenation, cerebral blood flow and cerebral blood volume responses during visual stimulation. Neuroimage 2008;43:1-9.

38) Hyder F. Dynamic imaging of brain function. Methods Mol Biol 2008;489:3-22.

39) Buxton RB, Wong EC, Frank LR. Dynamics of blood flow and oxygenation changes during brain activation: the balloon model. Magn Reson Med 1998;39:855-64.

40) Friston KJ, Price CJ. Dynamic representations and generative models of brain function. Brain Res Bull 2001;54:275-85.

41) Herman P, Trubel HK, Hyder F. A multiparametric assessment of oxygen efflux from the brain. J Cereb Blood Flow Metab 2006;26:79-91.

42) Huppert TJ, Allen MS, Benav H, Jones PB, Boas

DA. A multicompartment vascular model for inferring baseline and functional changes in cerebral oxygen metabolism and arterial dilation. J Cereb Blood Flow Metab 2007;27:1262-79.

43) Birn RM, Saad ZS, Bandettini PA. Spatial heterogeneity of the nonlinear dynamics in the FMRI BOLD response. Neuroimage 2001;14:817-26.

44) Glover GH. Deconvolution of impulse response in event-related BOLD fMRI. Neuroimage 1999;9: 416-29.

45) Norup Nielsen A, Lauritzen M. Coupling and uncoupling of activity-dependent increases of neuronal activity and blood flow in rat somatosensory cortex. J Physiol 2001;533:773-85.

46) Nemoto M, Sheth S, Guiou M, Pouratian N, Chen JW, Toga AW. Functional signal- and paradigm-dependent linear relationships between synaptic activity and hemodynamic responses in rat somatosensory cortex. J Neurosci 2004;24:3850-61.

47) Smith AJ, Blumenfeld H, Behar KL, Rothman DL, Shulman RG, Hyder F. Cerebral energetics and spiking frequency: the neurophysiological basis of fMRI. Proc Natl Acad Sci USA 2002;99:10765-70.

48) Maandag NJ, Coman D, Sanganahalli BG, et al. Energetics of neuronal signaling and fMRI activity. Proc Natl Acad Sci USA 2007;104:20546-51.

49) Masamoto K, Kim T, Fukuda M, Wang P, Kim SG. Relationship between neural, vascular, and BOLD signals in isoflurane-anesthetized rat somatosensory cortex. Cereb Cortex 2007;17:942-50.

50) Huttunen JK, Grohn O, Penttonen M. Coupling between simultaneously recorded BOLD response and neuronal activity in the rat somatosensory cortex. Neuroimage 2008;39:775-85.

51) Ureshi M, Matsuura T, Kanno I. Stimulus frequency dependence of the linear relationship between local cerebral blood flow and field potential evoked by activation of rat somatosensory cortex. Neurosci Res 2004;48:147-53.

52) Devor A, Dunn AK, Andermann ML, Ulbert I, Boas DA, Dale AM. Coupling of total hemoglobin concentration, oxygenation, and neural activity in rat somatosensory cortex. Neuron 2003;39:353-9.

53) Jones M, Hewson-Stoate N, Martindale J, Redgrave P, Mayhew J. Nonlinear coupling of neural activity and CBF in rodent barrel cortex. Neuroimage 2004;22:956-65.

54) Franceschini MA, Nissila I, Wu W, Diamond SG, Bonmassar G, Boas DA. Coupling between somatosensory evoked potentials and hemodynamic response in the rat. Neuroimage 2008;41: 189-203.

55) Pries AR, Ley K, Gaehtgens P. Generalization of the Fahraeus principle for microvessel networks. Am J Physiol 1986;251:H1324-32.

56) Fahraeus R. The suspension stability of the blood. Physiol Rev 1929;9:241-74.

57) Ebner FF, Armstrong-James MA. Intracortical processes regulating the integration of sensory information. Prog Brain Res 1990;86:129-41.